HHS Public Access

Author manuscript

Curr Biol. Author manuscript; available in PMC 2021 September 29.

Published in final edited form as:

Curr Biol. 2021 September 27; 31(18): 4148–4155.e4. doi:10.1016/j.cub.2021.06.089.

Thalamic input to motor cortex facilitates goal-directed action initiation

Naoya Takahashi[1,4,5,*], **Sara Moberg**[2], **Timothy A. Zolnik**[1], **Julien Catanese**[3], **Robert N.S. Sachdev**[1], **Matthew E. Larkum**[1], **Dieter Jaeger**[3,*]

[1]Institute for Biology, Humboldt University of Berlin, 10117 Berlin, Germany

[2]Einstein Center for Neurosciences Berlin, 10117 Berlin, Germany

[3]Department of Biology, Emory University, Atlanta, GA 30322, USA

[4]Present address: University of Bordeaux, CNRS, Interdisciplinary Institute for Neuroscience (IINS), UMR 5297, 33000 Bordeaux, France

[5]Lead contact

SUMMARY

Prompt execution of planned motor action is essential for survival. The interactions between frontal cortical circuits and the basal ganglia are central to goal-oriented action selection and initiation.[1–4] In rodents, the ventromedial thalamic nucleus (VM) is one of the critical nodes that conveys the output of the basal ganglia to the frontal cortical areas including the anterior lateral motor cortex (ALM).[5–9] Recent studies showed the critical role of ALM and its interplay with the motor thalamus in preparing sensory-cued rewarded movements, specifically licking.[10–12] Work in primates suggests that the basal ganglia output to the motor thalamus transmits an urgency or vigor signal,[13–15] which leads to shortened reaction times and faster movement initiation. As yet, little is known about what signals are transmitted from the motor thalamus to the cortex during cued movements and how these signals contribute to movement initiation. In the present study, we employed a tactile-cued licking task in mice while monitoring reaction times of the initial lick. We found that inactivation of ALM delayed the initiation of cued licking. Two-photon Ca^{2+} imaging of VM axons revealed that the majority of the axon terminals in ALM were transiently active during licking. Their activity was predictive of the time of the first lick. Chemogenetic and optogenetic manipulation of VM axons in ALM indicated that VM inputs facilitate the initiation of cue-triggered and impulsive licking in trained mice. Our results suggest that VM thalamocortical inputs increase the probability and vigor of initiating planned motor responses.

*Correspondence: naoya.takahashi@u-bordeaux.fr (N.T.), djaeger@emory.edu (D.J.).

AUTHOR CONTRIBUTIONS

N.T., R.N.S.S., M.E.L., and D.J. conceived the project and designed the experiments. N.T. performed *in vivo* experiments and data analysis. S.M. conducted histology and helped with behavioral training. T.A.Z. performed e*x vivo* electrophysiology experiments. J.C. performed *in vivo* electrophysiology experiments in VM. N.T., R.N.S.S., and D.J. wrote the paper with input from all authors.

DECLARATION OF INTERESTS

The authors declare no competing interests.

SUPPLEMENTAL INFORMATION

Supplemental information can be found online at https://doi.org/10.1016/j.cub.2021.06.089.

In brief

The ventromedial thalamus (VM) is a critical node mediating the basal ganglia-cortical interaction. In mice trained in a tactile-cued licking task, Takahashi et al. find a transient activation of VM axons in the premotor cortex preceding lick initiation. VM inputs modulate cortical activity and increase the probability and vigor of licking.

Graphical Abstract

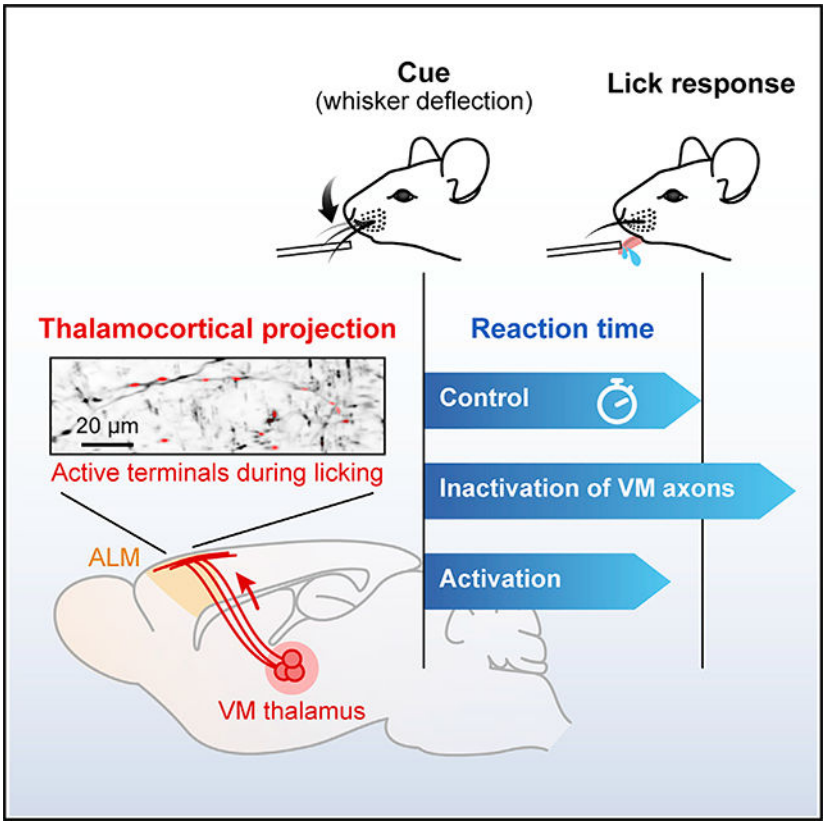

RESULTS

Initiation of cued licking depends on ALM activity

To study sensory-cued goal-directed action, we monitored lick initiation in mice performing a tactile detection task. Mice were trained to lick a water spout to obtain a water reward in response to deflection of a single whisker (Figures 1A and 1B).[16,17] A magnetic coil was used to deflect a small piece of metal tubing slid over the right C2 whisker. Once mice had learned the task, we varied the amplitude of the whisker deflection and plotted a psychometric curve (stimulus intensity versus detection probability) to determine the perceptual threshold for each mouse (Figure 1C). The threshold for stimulus detection was defined as the stimulus strength at which mice licked correctly on ~50% of the trials. The reaction time, defined as the time between whisker deflection and the animal's first lick, was longer in trials at the threshold intensity than those in trials at the 2-fold intensity of the

threshold (salient) (274 ± 39 ms versus 218 ± 34 ms, n = 18 sessions from six mice; Figure 1D).

The anterior lateral motor cortex (ALM) is essential for planning and executing goal-directed licking,[11,12,18,19] and bilateral inactivation of ALM causes severe impairment of learned lick responses in mice.[20–23] Here, we unilaterally inactivated the ALM contralateral (left) to the whisker stimulus in mice performing the detection task by injecting the $GABA_A$ receptor agonist, muscimol (Figures 1E and 1F). Muscimol did not change the overall probability of licking in response to whisker stimuli (Figure 1G), presumably due to the right ALM area, which remained active. However, the unilateral inactivation delayed the initiation of licking in hit trials, resulting in increased reaction times for both threshold (control versus muscimol: 303 ± 11 ms versus 362 ± 19 ms) and salient stimuli (260 ± 12 ms versus 339 ± 26 ms, n = 8 sessions from four mice, mean ± SEM; Figure 1H). Control experiments with saline injection in left ALM or muscimol injection in vibrissa M1 (vM1) did not affect the behavioral performance or alter the reaction time (Figure S1). Note that inactivation of left ALM only affected the reaction time and had no effect on the licking rate or pattern after the first lick (Figure 1I), indicating that ALM regulates the initiation of cued licking, not the coordination of a series of licks.

Robust, phasic motor thalamic input precedes sensory-cued licking

There is increasing evidence that the interaction between the motor thalamus and ALM is pivotal in goal-directed licking.[10,24] To directly measure thalamic inputs to ALM during cued licking, we performed two-photon Ca^{2+} imaging of axons of the ventromedial thalamic (VM) neurons. By injecting an AAV vector into the left VM (contralateral to the stimulated whisker), we expressed a genetically encoded Ca^{2+} indicator, GCaMP6s, in VM neurons and their axons (Figure 2A). GCaMP6s-expressing VM axons were abundant in L1 of the left frontal motor areas including ALM and vM1 (Figure 2B). We imaged VM axons in ALM through a chronic imaging window while the mice performed the detection task (Figure 2A, right). Ca^{2+} signals were measured from individual axonal boutons in L1 at ~30 frames/s over 240–540 trials per field of view (FOV; 134 × 134 μm^2) (Figure 2C). During imaging, mice received three types of stimuli: no stimulus (catch), threshold stimulus, and salient stimulus (Figure 2D). We found strong phasic activation of VM boutons in hit trials, i.e., when mice responded to a whisker deflection (Figure 2D, middle and right). Axonal signals also increased during false alarms, i.e., when mice licked even though no whisker-stimulus was present. In contrast, there was almost no activation of the boutons following whisker stimuli in miss trials. We quantified the activity of individual boutons by applying receiver operating characteristic (ROC) curve analysis to Ca^{2+} responses of each bouton to threshold stimuli (n = 856 boutons in 10 FOVs from five mice; Figure 2E). We calculated the area under the ROC curve (auROC; ranging from 0 to 1) to compare the likelihood that axonal Ca^{2+} signals are the same between hit versus miss trials (auROC = 0.5), higher for hit trials (auROC > 0.5), or less for hit trials (auROC < 0.5) (see STAR Methods). A majority (65.4%, 560/856 boutons) of VM axonal boutons in ALM showed reliable Ca^{2+} increases in hit trials (i.e., *auROC > 0.5 with $p < 0.05$), while a small fraction (7.8%, 67/856 boutons) were silenced during hit trials (i.e., *auROC < 0.5 with $p < 0.05$) (Figure 2E, right). We obtained similar results for VM boutons imaged in vM1 (n = 636 boutons in eight FOVs from six

mice; Figures S2A–S2E). There was no significant difference in auROC of boutons in ALM versus those in vM1 ($p = 0.81$, Mann-Whitney U test), implying a uniform function of VM input across frontal motor cortices[25] (but see Guo et al.[6]).

VM boutons in ALM with *auROC > 0.5 had faster onset of Ca^{2+} transients for salient stimuli than for threshold stimuli (310 ± 197 ms versus 362 ± 204 ms, n = 560 boutons; Figures 2F and 2G). This difference was diminished when evoked Ca^{2+} onset-transients were aligned to the first lick (50 ± 255 ms for salient stimuli and 38 ± 255 ms for threshold stimuli, n = 560 boutons; Figures 2H and 2I). The onsets of Ca^{2+} activity coincided with the animal's first lick, with some boutons activated up to 150 ms preceding the lick, while others were activated during licking. For individual VM boutons, Ca^{2+} onsets were variable in timing across trials. Nevertheless, the onset times of lick-preceding boutons were more precise, i.e., less variable, than those of lick-following boutons (Figure 2J). These results show that phasic VM inputs arrive in ALM shortly before the onset of licking in hit trials. This temporal relationship between activation of VM axonal activity and licking was also evident for false alarm licks in catch trials (Figures 2H and 2I). Note that in these analyses, the timing of VM inputs might be estimated slower than in reality due to the slow kinetics of GCaMP6s (rise time, ~150 ms).[26] Our results are in line with a recent electrophysiological study showing a ramping increase in VM single-unit activity before licking.[27]

To estimate the reliability of lick-associated VM inputs on individual trials, we trained linear classifiers to decode behavioral outcomes, i.e., hit or miss, from simultaneously imaged boutons. At the perceptual threshold, the classifier's performance increased before the lick initiation and reached almost 100% at peak (Figure 2K). The decoding performance was maintained by a few tens of boutons that were randomly selected to train the classifier (Figure 2L), implying that VM inputs carry reliable, robust lick-related information.

We also performed ROC analysis to test whether VM boutons encoded sensory variables, i.e., stimulus intensity (threshold versus salient stimuli). Interestingly, in 26.9% (230/855) of VM boutons in ALM during hit trials, Ca^{2+} responses to salient stimuli were significantly greater than those to threshold stimuli, indicating that VM inputs also vary across stimulus intensity.

Overall, our results indicate a strong correlation between VM inputs in ALM and the initiation of cued licking. But, notably, VM axons were also active during spontaneous licks to random rewards, independent of the task (Figure S2F–S2J). Single-unit recording from the VM thalamus showed that 55.8% (258/462) of VM neurons increased their activity during individual licks (other than the first lick within a typical water consumption lick train) at different phases of licking (Figure S2K). To examine whether VM activity was a signal that modulates the lick initiation or simply reflected the occurrence of licking, we next tested the causal influence of VM inputs on behavior.

Inactivation of VM inputs in ALM delays cued licking

To address whether VM inputs to ALM had a causal role in cued licking, we chemogenetically silenced VM inputs in ALM during the detection task. An inhibitory designer receptor exclusively activated by designer drug (DREADD), hM4Di, was virally

expressed in the left VM, contralateral to the stimulated whisker (Figure S3A). *Ex vivo* experiments confirmed potent chemogenetic silencing of synaptic transmission at hM4Di-expressing axon terminals. Photostimulation of VM axons co-expressing channelrhodopsin-2 (ChR2) and hM4Di evoked excitatory postsynaptic potentials (EPSPs) in ALM neurons, which were strongly suppressed in the presence of a hM4Di ligand, clozapine-n-oxide (CNO) (control versus CNO: 7.7 ± 2.3 mV versus 1.8 ± 0.4 mV, n = 11 neurons from three mice, mean ± SEM; Figures 3A and 3B). Local application of CNO into L1 of the left ALM i*n vivo* delayed the animals' lick response to salient whisker stimuli (236 ± 16 ms versus 264 ± 19 ms, n = 11 sessions from four mice, mean ± SEM; Figures 3C, 3D, and 3F), similar to the effect of muscimol in ALM (Figure 1). The probability of licking to whisker stimuli, however, remained unchanged (Figure 3E). CNO injection in control mice (not expressing hM4Di) did not affect behavioral performance (Figure S3B). Additionally, inactivation of VM inputs did not change the lick rate or the licking pattern (Figure 3G). These data support the idea that VM inputs modulate ALM to facilitate the initiation of sensory-cued lick responses.

Activation of VM inputs facilitates initiation of trained licking

To determine the impact of activation of VM inputs on lick initiation, we expressed ChR2 in VM neurons and photostimulated their axons in the left ALM with 470 nm light (20 Hz, 5 ms pulse width) (Figures 4A and S4A). Consistent with recent reports,[6,28] *ex vivo* photostimulation of VM axons in L1 evoked postsynaptic responses in both excitatory and inhibitory neurons in different layers of ALM (Figures S4B and S4C). In addition, *in vivo* photostimulation increased overall multi-unit activity in ALM (Figures 4B and 4C). Next, we photostimulated VM axons in mice performing the cued licking task (Figure 4D). Photostimulation, lasting throughout a trial, markedly increased spontaneous licking, seen as frequent timeouts ("lick early" trials) and an increase in false alarm rate (LED off versus LED on: 0.12 ± 0.03 versus 0.38 ± 0.05, n = 16 sessions from four mice, mean ± SEM; Figure 4E). This increased false alarm rate was accompanied by a reduction in perceptual gain (i.e., slope of the sigmoidally fitted psychometric function, 22.8 ± 10.2 versus 6.0 ± 1.6) but with no change in the perceptual threshold (0.68 ± 0.15 versus 0.60 ± 0.11, n = 16 sessions from four mice, mean ± SEM; Figures S4D–S4F). Moreover, there was a significant reduction in reaction time in trials with photostimulation (295 ± 13 ms versus 263 ± 10 ms for threshold stimuli; 257 ± 12 ms versus 240 ± 11 ms for salient stimuli, n = 16 sessions from four mice, mean ± SEM; Figure 4F).

Finally, we tested whether transient activation of VM axons alters licking behavior in general. Brief 100-ms photostimulation elicited false alarm licks in expert mice performing the task (Figures 4G and 4H, left). By contrast, the same photostimulation did not elicit licking in untrained (naive), water-deprived mice (Figure 4H, right). In this experiment, naive mice were given water rewards at random intervals. Although VM neurons transmit signals for individual licks (Figure S2K), photostimulation did not affect ongoing licking in hit trials in expert mice (Figure 4I). Thus, our results suggest that VM inputs specifically modulate trained goal-directed responses, which in previous studies has been found to be coded in ALM network activity.[10,12,22]

DISCUSSION

The VM thalamus is an essential waystation from the basal ganglia to the cortex.[5] Additionally, it receives inputs from the cerebellar nuclei[29–31] and other subcortical structures, notably the superior colliculus.[32,33] The thalamocortical projection from VM to cortical motor areas has been suggested to contribute to subcortical control of cortical activity during periods of movement preparation and initiation.[6,9] In the present study, we measured VM thalamocortical signals and performed optogenetic and chemogenetic manipulations to test the functional effect of this thalamocortical pathway on sensory-cued movements.

VM axons predominantly target layer 1 (L1) in the cortex,[33,25] where they contact the apical dendrites of layer 2/3 (L2/3) and layer 5 (L5) pyramidal neurons[6,34] as well as local inhibitory interneurons.[28,35] We found that the majority of VM axons in ALM were transiently active at the onset of licking following an instructional whisker stimulus. These axons were also active in false alarm trials. Photostimulation of VM axons increased impulsive licks, i.e., false alarm licks, in task-engaged mice. Interestingly, the same photostimulation, however, did not produce spontaneous licks in untrained, thirsty mice waiting for un-cued, random water rewards. This result agrees with a recent study showing the learning-dependent emergence of VM axonal activity for skilled movements.[9] Taken together, our results show that VM thalamocortical inputs facilitate the initiation of trained goal-directed movements. Transient, concerted activation of VM inputs may reorganize network activity in the motor cortex, converting preparatory activity to a command signal to execute movements.[11,36,37]

Chemogenetic inactivation of VM inputs to ALM increased the animal's reaction time, while optogenetic activation shortened it. These results are in line with the idea that the basal ganglia control movement vigor,[13,14] and activity in these circuits leads to acceleration of action release. Thus, our data suggest a role for the VM thalamocortical projection in integrating vigor signals with command signals at the cortical level for goal-directed movements. In the present study, we primarily targeted the VM thalamus, but the surrounding thalamic nuclei, including the ventral anterior and ventral lateral nuclei (VA/VL), also project to ALM. Although the viral expression was relatively well restricted to VM (Figures S3A and S4A), we cannot exclude contributions of other thalamocortical inputs in ALM to the obtained results. For example, the rostroventral part of VA/VL also receives inputs from the basal ganglia and has been implicated to functionally overlap with VM.[7]

Our results imply that the VM thalamus, a key target of the basal ganglia, links activity in the basal ganglia to L1 of the premotor cortex, where it modulates the initiation of movements. An inability to initiate movements, a cardinal symptom of Parkinson's disease, is thought to arise from increased inhibition of the motor thalamus by the basal ganglia.[38,39] Therefore, failure of signaling in the VM thalamocortical pathway could be central to movement disorders such as Parkinson's disease. Indeed, this hypothesis is supported by recent studies showing that inhibitory inputs from substantia nigra pars reticulata to the VM thalamus impede lick initiation in mice engaged in a directional licking task.[27,40]

STAR★METHODS

RESOURCE AVAILABILITY

Lead contact—Further information and requests for resources and reagents should be directed to and will be fulfilled by the lead contact, Naoya Takahashi (naoya.takahashi@u-bordeaux.fr).

Materials availability—This study did not generate new unique reagents.

Data and code availability—The data and MATLAB analysis code for generating the figures are available at the open access CERN Zenodo database (https://doi.org/10.5281/zenodo.5036596).

EXPERIMENTAL MODEL AND SUBJECT DETAILS

Animals—Adult C57BL/6J male mice (> P60) were used. Mice were housed in groups of 2–4 mice per cage in a 12:12 reversed day-night cycle. All experiments were conducted following the guideline given by Landesamt für Gesundheit und Soziales Berlin (LAGeSo) and were approved by this authority.

METHOD DETAILS

Cranial window implantation—During the surgery, mice were anesthetized with isoflurane (1.5%–2.0% in O_2) or ketamine (100 mg/kg)/xylazine (10 mg/kg) and kept on a thermal blanket. For *in vivo* two-photon Ca^{2+} imaging, AAV2/1-Syn-GCaMP6s-WPRE (Addgene) was injected through a glass pipette (tip diameter, 5–10 μm) into the left VM based on stereotaxic coordinates (1.5 mm posterior and 0.9 mm lateral from bregma). A single injection (100 nl) was made at a depth of 3.9 mm under the pia. Two weeks after the viral vector injection, the scalp and periosteum were carefully removed. A light-weight head-post was fixed on the skull over the right hemisphere with light-curing adhesives and dental cement. A 3-mm craniotomy was made over the frontal motor area in the left hemisphere of the mice. The craniotomy was sealed with a double-layered 3-mm glass coverslip with cyanoacrylate glue and dental cement. The double-layered glass was comprised of two 150-μm-thick glass coverslips cured together using UV curable adhesive (Norland Optical Adhesive 61). Imaging experiments began four weeks after the AAV injection. Imaging was performed in ALM (2.5 mm anterior and 1.5 mm lateral from bregma)[10,18] and vM1 (1.0 mm anterior and 1.0 mm lateral from bregma).

Behavior—Mice were kept on a reversed light/dark cycle. Habituation of the mice to head restraint began a week after the head-post or chronic window surgery. Head-restrained time on the first day was 5 min and then gradually increased each day until the mice sat calmly for 60 min. Mice were water restricted during subsequent periods of behavioral training.

Behavioral events (e.g., licking, whisker deflection, reward delivery) were monitored and controlled by a custom-written program running on a microcontroller board (Arduino), as previously described.[17,42] Briefly, the C2 whisker was deflected by displacing a light metal tube (~3 mg) slid over the whisker using a magnetic coil placed underneath the animal.

Local magnetic force was generated by loading the coil with a Gaussian-shaped current pulse (s = 3.4 ms). Mice were first trained to detect a relatively strong whisker deflection (~8°, ~1000°/s) delivered with a random inter-stimulus interval (6–8 s) to obtain a water reward. Impulsive licking in the 1.5 s (no-lick period) preceding the scheduled stimulus ("lick early") paused the trial and triggered a brief timeout (6–8 s). If the mice licked a water spout within a response window (from 0 to 0.7 s after the stimulus onset), a drop of water (~5 μl) was delivered through the spout. Mice learned the task within one to two weeks (false alarm rate: < 20%, hit rate: > 80%). We then tested the psychometric function of the mice by deflecting the C2 whisker at seven different amplitudes including no stimulus for catch trials. Whisker stimuli with different intensities were randomly interspersed in trials. For experiments with three stimulus conditions (i.e., no stimulus, threshold stimulus, salient stimulus), we chose the threshold intensity to yield ~50% detection performance.

Two-photon Ca^{2+} imaging—Imaging from behaving mice was performed with a resonant-scanning two-photon microscope (Thorlabs) equipped with GaAsP photomultiplier tubes (Hamamatsu). GCaMP6s was excited at 940 nm (typically 20–30 mW at the sample) with a Ti:Sapphire laser (Mai Tai eHP DeepSee, Spectra-Physics) and imaged through a 16 ×, 0.8 NA water-immersion objective (Nikon) and GaAsP PMTs (Hamamatsu). Full-frame images (512 × 512 pixels; pixel size, 0.26 × 0.26 μm^2) were acquired from VM axons expressing GCaMP6s at a depth of 20–40 μm at 30.3 Hz using ScanImage 4.1 software (Vidrio Technologies). On each trial, a sequence of 105 frames was acquired 1.50 s before (as baseline) and 1.97 s after (as response) the stimulus onset.

***In vivo* pharmacology—**A small hole was made over the left ALM or vM1 under brief anesthesia with isoflurane and covered with a silicone cap (Kwik-Cast) 60 min before experiments started. After a control session (60 trials), 2.4 μg/μl muscimol (100 nl at each depth; Tocris Bioscience) was injected through a glass pipette each at depths of 300 μm and 600 μm under the pia. Twenty min after the injection, the effect of muscimol on behavioral performance was tested in a new behavioral session (60 trials) with the same stimulus intensities. After the last session of the pharmacology experiment, fluorescent muscimol (BODIPY TMR-X conjugate, Thermo Fisher Scientific) was injected into the same injection site (100 nl each at depths of 300 μm and 600 μm), and mice were perfused 20 min after the injection.

***In vivo* chemogenetics—**AAV2/1-hSyn1-hM4D(Gi)-mCherry-WPRE (100 nl, Viral Vector Facility, University of Zurich) was injected into the left VM. Two weeks after the injection, a head-post was implanted with dental cement, leaving a small region of the skull over the left ALM exposed. Experiments began four weeks after the virus injection. A small hole was made over the left ALM under brief anesthesia with isoflurane and covered with Kwik-Cast 60 min before experiments started. After a control session (60 trials), 150 nl of 10 μM CNO (Tocris Bioscience) was injected into L1 through a glass pipette at a depth of 100 μm under the pia. Ten min after the injection, the effect of CNO on behavioral performance was tested in a new behavioral session (60 trials) with the same stimulus intensities.

***In vivo* optogenetics—**AAV2/1-hSyn-ChR2(H134R)-YFP-WPRE (100 nl, Addgene) was injected into the left VM. Two weeks after the injection, the skull over the left ALM was carefully thinned by drilling and covered with a thin layer of cyanoacrylate glue. A head-post was fixed on the skull in the right hemisphere with light-curing adhesives and dental cement. Optogenetic experiments began three weeks after the AAV injection. Photostimulation light (470 nm, 1.0–2.5 mW) was locally delivered to the left ALM via an optic fiber (200 μm in diameter, 0.39 NA, Thorlabs), placed over the thinned skull window. For constant activation of VM axons, photostimulation (5-ms-light pulses at 20 Hz) started 0.5 s before whisker stimulation and lasted for 1.5 s. For brief photostimulation, three light pulses (5 ms, 20 Hz) were delivered in catch trials or at 0.7 s after the stimulus onset in hit trials (i.e., while mice were licking). In order to prevent the mice from distinguishing photostimulation trials from control trials using visual cues, the optic fiber and the optical windows were enclosed in a black rubber cap to prevent light leakage from photostimulation into the animals' eyes. Additionally, a masking light was continuously delivered onto the eyes via a 470 nm LED.

Note that although the ChR2-YFP expression was relatively well restricted to VM (Figure S4A), there were some spreads of expression in VA/VL, which also projects to ALM (preferentially to deeper layers[25]). Thus, we cannot exclude the possibility that some VA/VL axons may have been photostimulated in these experiments.

***In vivo* electrophysiology—**For MUA recording from ALM, a small craniotomy (diameter, ~300 μm) was made over the left ALM in mice injected with AAV2/1-hSyn-ChR2(H134R)-YFP-WPRE. The craniotomy was kept moist with artificial cerebrospinal fluid (ACSF; 125 mM NaCl, 25 mM $NaHCO_3$, 2.5 mM KCl, 1.25 mM NaH_2PO_4, 1 mM $MgCl_2$, 25 mM glucose and 2 mM $CaCl_2$). A single tungsten microelectrode (~0.5 MΩ, FHC) was inserted through the craniotomy at a depth of 300 and 600 μm from the pial surface. Signals were amplified and band-pass filtered (0.3–5 kHz) with an extracellular amplifier (EXT-02B, NPI Electronic) and sampled at 25 kHz with a Power1401 data acquisition interface using Spike2 software (CED).

For single-unit recording from VM, a small craniotomy was made over the left VM a few days before recording. Signals were obtained by acute insertion of silicon probes made four shanks separated by 200 μm with eight channels per shank separated by 100 μm (A4×87mm-100–200-177, Neuronexus Inc) and sampled at 20 kHz with an RHD2000 recording system (Intan Technologies). Single unit spikes were extracted and sorted using an offline spike-sorting program (Wave Clus).[41] In this experiment, mice performed a directional licking task used in our recent study.[27]

***Ex vivo* electrophysiology—**Mice injected with AAV2/1-hSyn-ChR2(H134R)-YFP-2a-hM4Di-WPRE (Charité Viral Core Facility) in VM were anesthetized with isoflurane before decapitation. The brain was then rapidly transferred to ice-cold, oxygenated cutting solution containing 110 mM choline chloride, 26 mM $NaHCO_3$, 2.5 mM KCl, 1.25 mM NaH_2PO_4, 11.6 mM sodium ascorbate, 3.1 mM sodium pyruvate, 7 mM $MgCl_2$, 0.5 mM $CaCl_2$, and 10 mM glucose (pH 7.4). Coronal slices (300 μm thick) were cut in an ice-cold solution using a vibratome (VT1200 S, Leica). Slices were incubated in the same solution at 32°C for 5

min, and then transferred to ACSF (pH 7.4) for an additional 25 min at 32°C and then kept at room temperature (RT) before use for recording.

Somatic whole-cell recordings were obtained from neurons in ALM. Recording pipettes (4–8 ΩW) were filled with an intracellular solution containing 115 mM K-gluconate, 5 mM KCl, 10 mM HEPES, 10 mM Na_2-phosphocreatine, 4 mM Mg-ATP, 0.3 mM GTP, and 0.1% biocytin (pH 7.25–7.3, 285–295 mOsm). Signals were amplified with a BVC-700A amplifier (Dagan) and digitized at 20 kHz by an analog-digital converter (ITC-18, HEKA Elektronik). Acquisition was performed using custom-written IGOR Pro software. No correction was made for the junction potential between the bath and pipette solutions.

Photostimulation light (470 nm, UHP-T-470-SR, Prizmatix) was delivered to L1 through an iris and 60 × water-immersion objective (Olympus). The resulting area of direct illumination was ~50 μm in diameter. The power output at the objective was ~40 mW/mm^2. We stimulated with three 5 ms light pulses at 20 Hz with an interval of 10 s, and averaged > 20 trials for analysis. 10 μM CNO was perfused in the bath for > 5 min before measuring the effect of CNO.

Histology—Mice were anesthetized using isoflurane (1.5%–2% in O_2) and euthanized by an intraperitoneal injection of urethane (1.5 g/kg). Mice were perfused transcardially with 0.1 M phosphate buffered saline (PBS), followed by 4% paraformaldehyde (PFA) in PBS. After perfusion, brains were removed from the skull and postfixed in PFA overnight. The next day, brains were washed in PBS, transferred into a 30% sucrose solution in PBS, and left for at least 24 h for cryoprotection. For cryosectioning, brains were embedded in optimal cutting temperature compound. Coronal brain sections (60 μm) were incubated with blocking solution (2.5% bovine serum albumin, 0.3% Triton X-100 in 0.1M PBS) for 30 min at RT. For enhancement of GCaMP6s signals, sections were incubated in primary antibody against GFP (chicken; 1:5000, GeneTex) for 12 h at RT. Sections were then washed in PBS followed by incubation in Alexa Fluor 488 donkey anti-chicken (1:500, Jackson ImmunoResearch) for 2 h at RT. Next, sections were washed, and nuclei were counterstained with NucBlue (Thermo Fisher Scientific) for 5 min at RT. After washing, sections were mounted on slides and coverslipped using Fluoromount-G mounting medium. Images were obtained using a fluorescent microscope (DMI 4000 B, Leica Microsystems) equipped with 2.5 × and 10 × air objectives.

After *ex vivo* recordings, slices were kept in 4% PFA in PBS overnight. Biocytin-filled neurons were stained using Alexa Fluor 647-conjugated streptavidin (1:1000, Thermo Fisher Scientific). Sections were washed four times for 1 h in 0.1 M phosphate buffered (PB; pH 7.23–7.25) on a rotating table at RT. Next, sections were incubated with Streptavidin in staining buffer (0.1% Triton X-100 in 0.1 M PB) first 1–2 h at RT, then 72 h at 4°C. The sections were then washed in 0.1 M PB four times for 1 h and mounted on glass slides with custom-made spacers and coverslipped using Fluoromount-G mounting medium (SouthernBiotech). Streptavidin-stained sections were visualized with Olympus FB1000 confocal microscope using a 30 × oil-immersion objective. Reconstruction of neuronal morphologies was done using neuTube software.[43]

QUANTIFICATION AND STATISTICAL ANALYSIS

All analysis was performed using ImageJ and custom-written code in MATLAB. Unless otherwise indicated, data in the text are reported as mean ± SD For statistics, data were first subjected to a Shapiro-Wilk test of normality and, based on its result, to the indicated parametric and non-parametric tests (two-sided). No statistical methods were used to predetermine sample sizes, but our sample sizes were similar to those reported in previous publications in the field.[9,12,20] Data collection and analysis were not performed blind to the conditions of the experiments.

Imaging data analysis—Lateral drifts of imaging frames due to animal motion were corrected by registering each frame to a reference image based on whole-frame cross-correlation. The reference image was obtained by averaging any given ten consecutive frames in which motion drifts were minimal. Acquisitions with major axial (in z) movement artifacts were rejected (4 /18 sessions). Regions of interest (ROIs) for VM axons were manually selected with the help of average intensity and standard deviation projections across movie frames. For each ROI, the time series of raw fluorescence was estimated by averaging all pixels within the ROI. Fluorescence change ($\Delta F/F_0$) was calculated as ($F - F_0$)/F_0, where F_0 was the mode of the fluorescence intensity histogram derived from the whole imaging session. The onsets of Ca^{2+} responses were determined as the times when the Ca^{2+} signals exceeded three times the standard deviation of their baseline fluctuations.

Behavioral performance analysis—Psychometric parameters, i.e., detection threshold and gain (slope), were estimated by fitting detection performance across stimulus intensities (7 intensities including no stimulus) with a logistic function:

$$P(x; \alpha, \beta, \gamma, \lambda) = \gamma + \frac{1 - \gamma - \lambda}{1 + e^{-\beta(x - \alpha)}}$$

where x is stimulus intensity, $P(x)$ is the detection probability, i.e., the fraction of hit or false alarm trials, and α, β, γ, λ are free parameters that were fitted using a maximum likelihood method. Parameter α and β measure the threshold intensity and slope of the psychometric function.

Receiver operating characteristic (ROC) and decoding analysis—ROC analysis was performed to quantify the response strength of individual axonal boutons to threshold stimuli between hit and miss trials. Mean axonal Ca^{2+} changes ($\Delta F/F_0$) within the 1.5 s following the stimulus were used for this analysis. For each bouton, the ROC curve was then obtained by plotting, for all criterion response levels, the fraction of hit trials in which the response exceeded the criterion against the fraction of miss trials in which the response exceeded the criterion. We then computed the area under the ROC curve (auROC) to quantify the performance of an ideal observer in categorizing trials into hit or miss based on the Ca^{2+} responses. The auROC ranges from 0 to 1, where the value of < 0.5 means "negative responses in hit trials," > 0.5 means "positive responses in hit trials," and 0.5 represents "no difference in responses between hit and miss trials." Statistical significance of the auROC was assessed by a permutation test, for which the sampling distribution

was obtained from 10,000 resampled datasets by exchanging labels (“hit” or “miss”) on trials. We also performed the same analysis on the Ca^{2+} responses within the 0.27 s (mean reaction) following the threshold stimuli. With this time window, 13.6% (116/856) of VM axonal boutons significantly increased Ca^{2+} activity in hit trials compared to miss trials. Note that this number may be underestimated due to the slow kinetics of GCaMP6s (rise time, ~150 ms) used in this study. Thus, there were likely many false negatives in the analysis with the time window of 0.27 s.

We also used ROC analysis to quantify the response strength of individual axonal boutons across stimulus intensities (threshold versus salient stimuli). For each bouton, the ROC curve was obtained by plotting, for all criterion response levels, the fraction of salient stimulus trials in which the response exceeded the criterion against the fraction of threshold stimulus trials in which the response exceeded the criterion.

To test whether the population activity of VM axonal boutons can predict the behavioral outcomes (i.e., hit or miss) in threshold stimulus trials, we performed decoding analysis on Ca^{2+} imaging data using a linear SVM decoder. The decoder was trained under a cross-validation procedure: for each experimental session, threshold stimulus trials were randomly partitioned into 70% training data and 30% testing data. Training data was constructed from the set of $N \times 1$ (N = axonal boutons) population activity vectors at a given time point. Decoder performance was evaluated on the testing data. This procedure was repeated 100 times, each time with a different set of training and testing data, to obtain averaged decoding accuracy. In order to estimate decoder performance preceding the first lick, population vectors for miss trials were sampled before and after the mean reaction time (0.27 s).

Supplementary Material

Refer to Web version on PubMed Central for supplementary material.

ACKNOWLEDGMENTS

This study was supported by the University of Bordeaux (Initiative of Excellence to N.T.), the Region Nouvelle-Aquitaine (to N.T.), the ATIP-Avenir program (to N.T.), the Einstein Center for Neurosciences Berlin (PhD fellowship to S.M.), the Deutsche Forschungsgemeinschaft (Exc 257 NeuroCure, LA 3442/3–1, LA 3442/6–1, project number 327654276 SFB1315 to M.E.L.), the European Union Horizon 2020 Research and Innovation Programme (72070/HBP SGA1, 785907/HBP SGA2, 670118/ERC ActiveCortex to M.E.L.), the Einstein Foundation Berlin (EVF-2017–363 to D.J.), and the NINDS (1UO1NS094302, R01NS111470 to D.J.). We thank the colleagues of the Research Workshop at the Charité - Universitätsmedizin Berlin for developing and manufacturing the experimental devices.

REFERENCES

1. Graybiel AM (2000). The basal ganglia. Curr. Biol 10, R509–R511. [PubMed: 10899013]
2. Hikosaka O, Nakamura K, Sakai K, and Nakahara H (2002). Central mechanisms of motor skill learning. Curr. Opin. Neurobiol 12, 217–222. [PubMed: 12015240]
3. Middleton FA, and Strick PL (2000). Basal ganglia and cerebellar loops: motor and cognitive circuits. Brain Res. Brain Res. Rev 31, 236–250. [PubMed: 10719151]
4. Parent A, and Hazrati LN (1995). Functional anatomy of the basal ganglia. I. The cortico-basal ganglia-thalamo-cortical loop. Brain Res. Brain Res. Rev 20, 91–127. [PubMed: 7711769]

5. Bosch-Bouju C, Hyland BI, and Parr-Brownlie LC (2013). Motor thalamus integration of cortical, cerebellar and basal ganglia information: implications for normal and parkinsonian conditions. Front. Comput. Neurosci 7, 163. [PubMed: 24273509]
6. Guo K, Yamawaki N, Svoboda K, and Shepherd GMG (2018). Anterolateral Motor Cortex Connects with a Medial Subdivision of Ventromedial Thalamus through Cell Type-Specific Circuits, Forming an Excitatory Thalamo-Cortico-Thalamic Loop via Layer 1 Apical Tuft Dendrites of Layer 5B Pyramidal Tract Type Neurons. J. Neurosci 38, 8787–8797. [PubMed: 30143573]
7. Kuramoto E, Fujiyama F, Nakamura KC, Tanaka Y, Hioki H, and Kaneko T (2011). Complementary distribution of glutamatergic cerebellar and GABAergic basal ganglia afferents to the rat motor thalamic nuclei. Eur. J. Neurosci 33, 95–109. [PubMed: 21073550]
8. Sieveritz B, García-Muñoz M, and Arbuthnott GW (2019). Thalamic afferents to prefrontal cortices from ventral motor nuclei in decision-making. Eur. J. Neurosci 49, 646–657. [PubMed: 30346073]
9. Tanaka YH, Tanaka YR, Kondo M, Terada SI, Kawaguchi Y, and Matsuzaki M (2018). Thalamocortical Axonal Activity in Motor Cortex Exhibits Layer-Specific Dynamics during Motor Learning. Neuron 100, 244–258.e12. [PubMed: 30174116]
10. Guo ZV, Inagaki HK, Daie K, Druckmann S, Gerfen CR, and Svoboda K (2017). Maintenance of persistent activity in a frontal thalamocortical loop. Nature 545, 181–186. [PubMed: 28467817]
11. Li N, Chen TW, Guo ZV, Gerfen CR, and Svoboda K (2015). A motor cortex circuit for motor planning and movement. Nature 519, 51–56. [PubMed: 25731172]
12. Guo ZV, Li N, Huber D, Ophir E, Gutnisky D, Ting JT, Feng G, and Svoboda K (2014). Flow of cortical activity underlying a tactile decision in mice. Neuron 81, 179–194. [PubMed: 24361077]
13. Cisek P, Puskas GA, and El-Murr S (2009). Decisions in changing conditions: the urgency-gating model. J. Neurosci 29, 11560–11571. [PubMed: 19759303]
14. Thura D, and Cisek P (2017). The Basal Ganglia Do Not Select Reach Targets but Control the Urgency of Commitment. Neuron 95, 1160–1170.e5. [PubMed: 28823728]
15. Turner RS, and Desmurget M (2010). Basal ganglia contributions to motor control: a vigorous tutor. Curr. Opin. Neurobiol 20, 704–716. [PubMed: 20850966]
16. Takahashi N, Ebner C, Sigl-Glöckner J, Moberg S, Nierwetberg S, and Larkum ME (2020). Active dendritic currents gate descending cortical outputs in perception. Nat. Neurosci 23, 1277–1285. [PubMed: 32747790]
17. Takahashi N, Oertner TG, Hegemann P, and Larkum ME (2016). Active cortical dendrites modulate perception. Science 354, 1587–1590. [PubMed: 28008068]
18. Chen TW, Li N, Daie K, and Svoboda K (2017). A Map of Anticipatory Activity in Mouse Motor Cortex. Neuron 94, 866–879.e4. [PubMed: 28521137]
19. Esmaeili V, Tamura K, Muscinelli SP, Modirshanechi A, Boscaglia M, Lee AB, Oryshchuk A, Foustoukos G, Liu Y, Crochet S, et al. (2021). Rapid suppression and sustained activation of distinct cortical regions for a delayed sensory-triggered motor response. Neuron 109, 2183–2201.e9. [PubMed: 34077741]
20. Komiyama T, Sato TR, O'Connor DH, Zhang YX, Huber D, Hooks BM, Gabitto M, and Svoboda K (2010). Learning-related fine-scale specificity imaged in motor cortex circuits of behaving mice. Nature 464, 1182–1186. [PubMed: 20376005]
21. Goard MJ, Pho GN, Woodson J, and Sur M (2016). Distinct roles of visual, parietal, and frontal motor cortices in memory-guided sensorimotor decisions. eLife 5, e13764. [PubMed: 27490481]
22. Li N, Daie K, Svoboda K, and Druckmann S (2016). Robust neuronal dynamics in premotor cortex during motor planning. Nature 532, 459–464. [PubMed: 27074502]
23. Allen WE, Kauvar IV, Chen MZ, Richman EB, Yang SJ, Chan K, Gradinaru V, Deverman BE, Luo L, and Deisseroth K (2017). Global Representations of Goal-Directed Behavior in Distinct Cell Types of Mouse Neocortex. Neuron 94, 891–907.e6. [PubMed: 28521139]
24. Gao Z, Davis C, Thomas AM, Economo MN, Abrego AM, Svoboda K, De Zeeuw CI, and Li N (2018). A cortico-cerebellar loop for motor planning. Nature 563, 113–116. [PubMed: 30333626]
25. Kuramoto E, Ohno S, Furuta T, Unzai T, Tanaka YR, Hioki H, and Kaneko T (2015). Ventral medial nucleus neurons send thalamocortical afferents more widely and more preferentially to layer 1 than neurons of the ventral anterior-ventral lateral nuclear complex in the rat. Cereb. Cortex 25, 221–235. [PubMed: 23968832]

26. Chen TW, Wardill TJ, Sun Y, Pulver SR, Renninger SL, Baohan A, Schreiter ER, Kerr RA, Orger MB, Jayaraman V, et al. (2013). Ultrasensitive fluorescent proteins for imaging neuronal activity. Nature 499, 295–300. [PubMed: 23868258]
27. Catanese J, and Jaeger D (2021). Premotor Ramping of Thalamic Neuronal Activity Is Modulated by Nigral Inputs and Contributes to Control the Timing of Action Release. J. Neurosci 41, 1878–1891. [PubMed: 33446518]
28. Anastasiades PG, Collins DP, and Carter AG (2021). Mediodorsal and Ventromedial Thalamus Engage Distinct L1 Circuits in the Prefrontal Cortex. Neuron 109, 314–330.e4. [PubMed: 33188733]
29. Chevalier G, and Deniau JM (1982). Inhibitory nigral influence on cerebellar evoked responses in the rat ventromedial thalamic nucleus. Exp. Brain Res 48, 369–376. [PubMed: 7151930]
30. Deniau JM, Kita H, and Kitai ST (1992). Patterns of termination of cerebellar and basal ganglia efferents in the rat thalamus. Strictly segregated and partly overlapping projections. Neurosci. Lett 144, 202–206. [PubMed: 1279485]
31. Gornati SV, Schäfer CB, Eelkman Rooda OHJ, Nigg AL, De Zeeuw CI, and Hoebeek FE (2018). Differentiating Cerebellar Impact on Thalamic Nuclei. Cell Rep. 23, 2690–2704. [PubMed: 29847799]
32. Krout KE, Loewy AD, Westby GW, and Redgrave P (2001). Superior colliculus projections to midline and intralaminar thalamic nuclei of the rat. J. Comp. Neurol 431, 198–216. [PubMed: 11170000]
33. Herkenham M (1979). The afferent and efferent connections of the ventromedial thalamic nucleus in the rat. J. Comp. Neurol 183, 487–517. [PubMed: 759445]
34. Collins DP, Anastasiades PG, Marlin JJ, and Carter AG (2018). Reciprocal Circuits Linking the Prefrontal Cortex with Dorsal and Ventral Thalamic Nuclei. Neuron 98, 366–379.e4. [PubMed: 29628187]
35. Cruikshank SJ, Ahmed OJ, Stevens TR, Patrick SL, Gonzalez AN, Elmaleh M, and Connors BW (2012). Thalamic control of layer 1 circuits in prefrontal cortex. J. Neurosci 32, 17813–17823. [PubMed: 23223300]
36. Kaufman MT, Churchland MM, Ryu SI, and Shenoy KV (2014). Cortical activity in the null space: permitting preparation without movement. Nat. Neurosci 17, 440–448. [PubMed: 24487233]
37. Svoboda K, and Li N (2018). Neural mechanisms of movement planning: motor cortex and beyond. Curr. Opin. Neurobiol 49, 33–41. [PubMed: 29172091]
38. Albin RL, Young AB, and Penney JB (1989). The functional anatomy of basal ganglia disorders. Trends Neurosci. 12, 366–375. [PubMed: 2479133]
39. DeLong MR (1990). Primate models of movement disorders of basal ganglia origin. Trends Neurosci. 13, 281–285. [PubMed: 1695404]
40. Morrissette AE, Chen PH, Bhamani C, Borden PY, Waiblinger C, Stanley GB, and Jaeger D (2019). Unilateral Optogenetic Inhibition and Excitation of Basal Ganglia Output Affect Directional Lick Choices and Movement Initiation in Mice. Neuroscience 423, 55–65. [PubMed: 31705892]
41. Quiroga RQ, Nadasdy Z, and Ben-Shaul Y (2004). Unsupervised spike detection and sorting with wavelets and superparamagnetic clustering. Neural Comput. 16, 1661–1687. [PubMed: 15228749]
42. Micallef AH, Takahashi N, Larkum ME, and Palmer LM (2017). A Reward-Based Behavioral Platform to Measure Neural Activity during Head-Fixed Behavior. Front. Cell. Neurosci 11, 156. [PubMed: 28620282]
43. Feng L, Zhao T, and Kim J (2015). neuTube 1.0: A New Design for Efficient Neuron Reconstruction Software Based on the SWC Format. eNeuro 2, NEURO.0049–14.2014.

Highlights

- Ventromedial (VM) thalamus targets layer 1 of anterior lateral motor cortex (ALM)
- VM axons in ALM are transiently active during initiation of cued licking
- Inactivation of VM axons delays initiation of cued licking
- Activation of VM axons shortens reaction time and increases impulsive licks

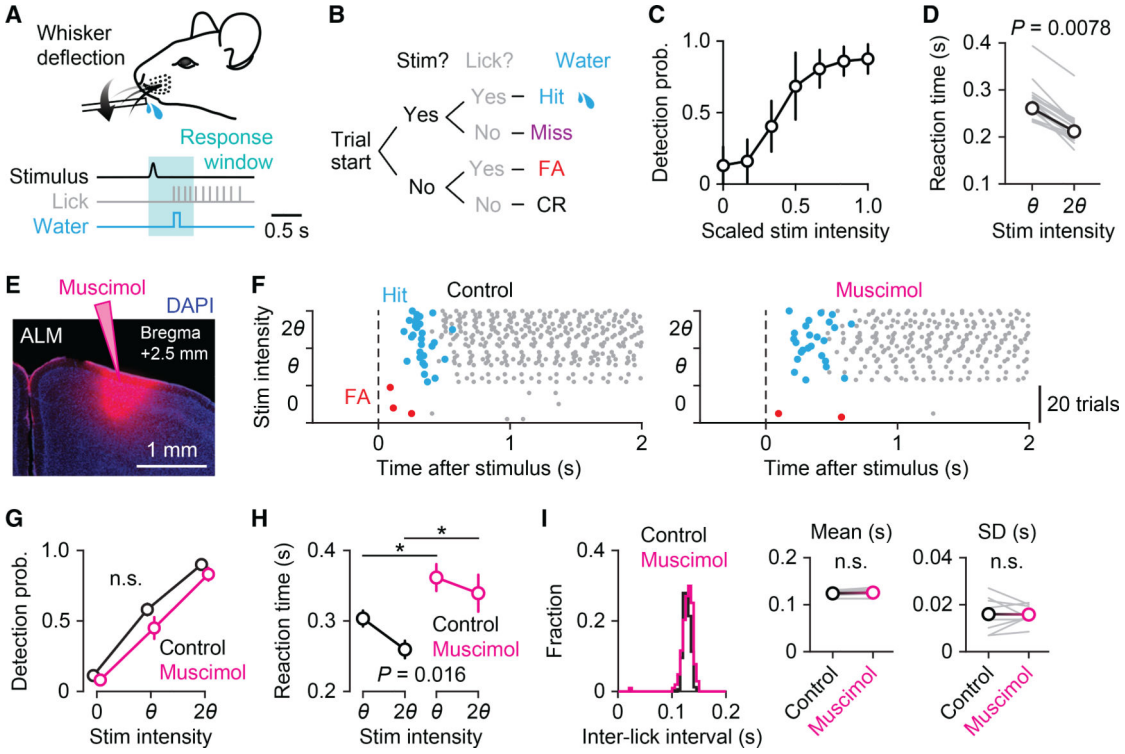

Figure 1. ALM is involved in lick initiation in a cued licking task

(A) Behavioral task design. Mice were trained to detect whisker deflections and lick a spout to obtain water rewards.

(B) Block diagram of the sequence of events for a single trial. Behavioral outcomes were classified into hit, miss, false alarm (FA), and correct rejection (CR).

(C) Psychometric function averaged across sessions (n = 20 sessions from four mice, mean ± SD).

(D) Reaction times for threshold (θ) and salient (twice the threshold intensity, 2θ) stimuli (n = 18 sessions from six mice; Wilcoxon signed-rank test). The gray lines represent individual sessions, and the black line represents the average.

(E) Site of infusion and diffusion of unilateral muscimol injection in ALM.

(F) Raster plot showing lick responses (gray dots) throughout a representative behavioral session before (left) and after (right) muscimol injection. The three stimulus types (catch, 0; threshold stimulus, θ; salient stimulus, 2θ) are randomly presented during the session but grouped here for plotting. Hit (rewarded) licks and FA licks are marked in blue and red, respectively.

(G–I) Behavioral comparisons before (black) and after (magenta) muscimol injection. (G) Detection probability (n = 8 sessions from four mice, mean ± SEM; p = 0.13, two-way repeated-measure ANOVA). (H) Reaction times for threshold and salient stimuli (n = 8 sessions from four mice, mean ± SEM; two-way repeated-measure ANOVA with Tukey-Kramer post hoc comparisons, *p = 0.046 for θ; *p = 0.018 for 2θ). (I) Histograms of inter-lick intervals in an example session (left). Insets: means (middle) and SDs (right) of inter-lick intervals (n = 8 sessions from four mice; p = 0.10 for means, p = 0.94 for SDs, paired t test).

See also Figure S1.

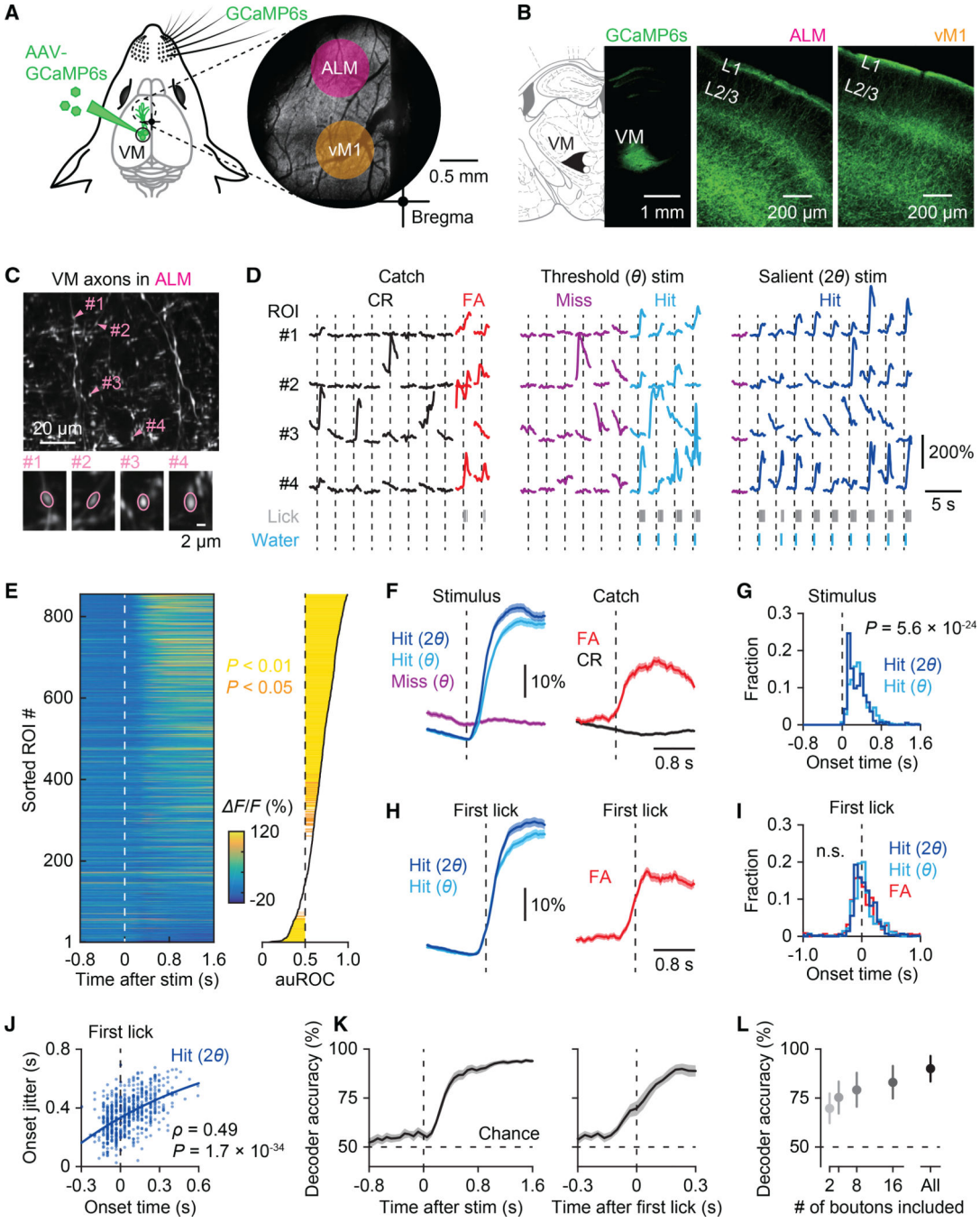

Figure 2. Transient activation of thalamocortical inputs in ALM coincides with lick initiation

(A) Left: Schematic of injection of AAV-GCaMP6s in the VM thalamus. Right: Two-photon image of GCaMP6s-expressing VM axons in L1 in the frontal motor areas through a chronic window.

(B) GCaMP6s expression in VM (left) and their axonal fibers in ALM (middle) and vM1 (right).

(C) Top: Two-photon image of a representative field of view showing VM axons in ALM. Bottom: Example axonal boutons indicated in the top panel.

(D) Example Ca^{2+} traces from the four boutons marked in (C) in catch (no stimulus) trials (left) and cued trials with threshold (θ; middle) or salient stimuli (2θ; right) (10 trials for each stimulus type). Trials were separated based on the animal's response; false alarm (FA) versus correct rejection (CR) for catch trials and hit versus miss for cued trials.
(E) Left: Ca^{2+} signals averaged across hit trials in response to threshold whisker stimuli. Right: Hit versus miss response strength of each bouton, calculated as the area under the ROC curve (auROC) (see STAR Methods). Boutons were sorted by auROC. Statistical significance is indicated in colors.
(F) Left: Ca^{2+} responses to salient stimuli and threshold stimuli in hit trials versus threshold stimuli in miss trials for axonal boutons that were positively correlated with behavior (*auROC > 0.5, $p < 0.05$) (n = 560 boutons, mean ± SEM). Right: Ca^{2+} activity associated with false alarm (red) versus correct rejection (black) in catch trials.
(G) Histogram of onset timings of Ca^{2+} responses in hit trials (n = 560 boutons; Wilcoxon singed-rank test).
(H) Ca^{2+} responses of axonal boutons with *auROC > 0.5 aligned by the timing of the first lick in hit (left) and false alarm trials (right) (n = 560 boutons, mean ± SEM).
(I) Histogram of onset timings of Ca^{2+} responses aligned by the first lick in hit and false alarm trials (n = 560 boutons for hit trials and 473 boutons for false alarm trials; $p = 0.47$, Kruskal-Wallis test).
(J) Correlation between the mean onset timing and the jitter (standard deviation) of Ca^{2+} responses aligned by the first lick in hit trials with salient stimuli (n = 554 boutons; Spearman's rank correlation). Each dot represents an axonal bouton with *auROC > 0.5.
(K) Left: Performance of a linear population classifier in decoding behavioral outcomes based on VM axonal activity (n = 10 sessions, mean ± SEM). Right: Decoder performance before and after the first lick (n = 10 sessions; $p = 4.9 \times 10^{-4}$ at 0 s, paired t test).
(L) Classifier performance at the end of the response time window (0.7 s after the stimulus) as a function of the number of boutons used to train decoders (n = 10 sessions, mean ± SD). See also Figure S2.

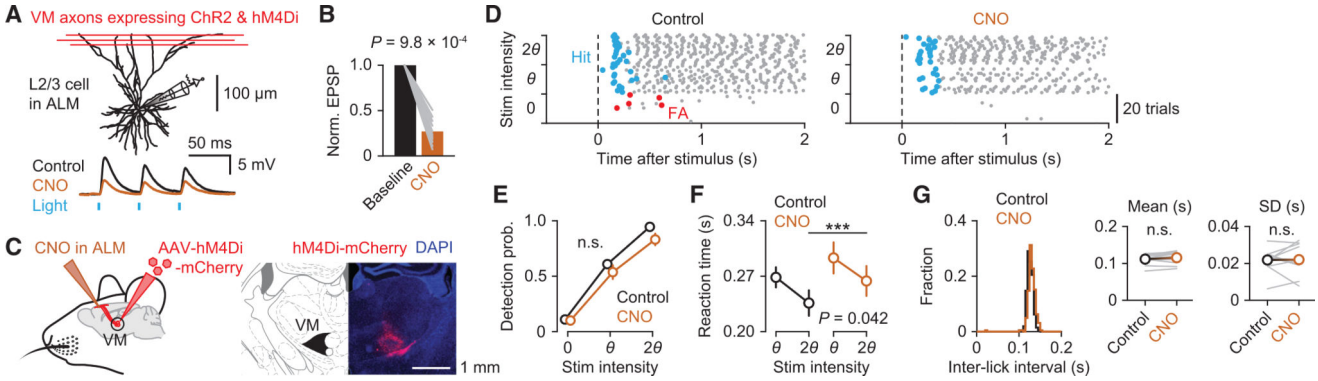

Figure 3. Inactivation of VM input delays initiation of cued licking

(A) Top: Reconstruction of a whole-cell recorded L2/3 pyramidal neuron in an ALM slice. Bottom: Excitatory postsynaptic potentials (EPSPs; average of 20 trials) in response to photostimulation (blue line) of VM axons co-expressing ChR2 and hM4Di in the absence (black) and presence (brown) of CNO.

(B) Normalized amplitudes of photostimulated EPSPs before and after bath application of CNO (n = 11 neurons from three mice; Wilcoxon singed-rank test).

(C) Left: Schematic showing inactivation of VM axon terminals expressing hM4Di by local application of CNO in ALM. Right: Expression of hM4Di-mCherry in VM.

(D) Raster plot showing lick responses (gray dots) throughout a representative behavioral session before (left) and after (right) local CNO injection. Hit (rewarded) licks and FA licks are marked in blue and red, respectively.

(E–G) Behavioral comparisons before (black) and after (brown) CNO injection. (E) Detection probability (n = 11 sessions from four mice, mean ± SEM; p = 0.35, two-way repeated-measure ANOVA). (F) Reaction times for threshold and salient stimuli (n = 11 sessions from four mice, mean ± SEM; two-way repeated-measure ANOVA with Tukey–Kramer post hoc comparisons, ***$p = 2.9 \times 10^{-4}$ for 2θ). (G) Histograms of inter-lick intervals in an example session (left). Insets: Means (middle) and SDs (right) of inter-lick intervals (n = 11 sessions from four mice; p = 0.078 for means, p = 0.94 for SDs, paired t test).

See also Figure S3.

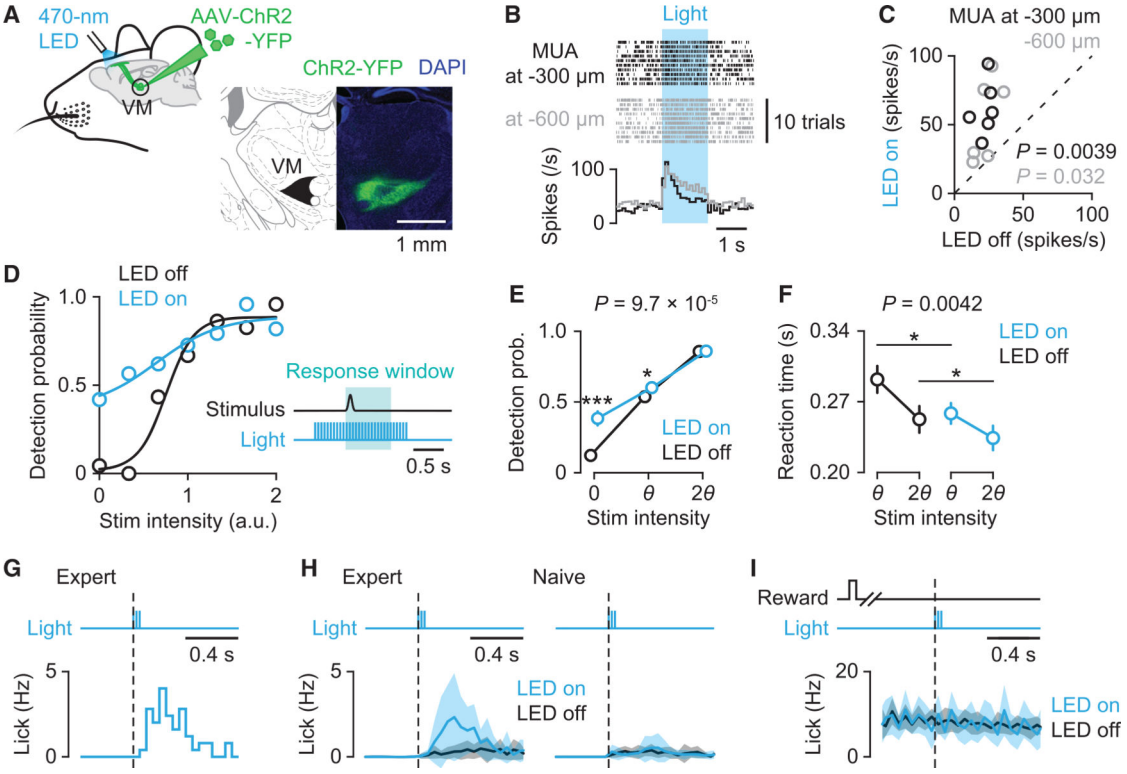

Figure 4. VM axon activation facilitates lick initiation by activating ALM

(A) Left: Schematic showing optogenetic stimulation of ChR2-expressing VM axons in ALM. Right: ChR2-YFP expression in VM.

(B) Raster plot (top) and peri-stimulus time histogram (PSTH) (bottom) of multi-unit activity (MUA) in ALM at 300 µm (black) and 600 µm (gray) below the pia during photostimulation (blue).

(C) Relationship between MUAs during control (LED off) and photostimulation (LED on) conditions (n = 6 recording sites for each depth from four mice; paired t test).

(D) Example of psychometric performance with (blue) or without (black) photostimulation of VM axons. Inset: Schematic showing the time course of photostimulation. 470 nm light (5 ms duration at 20 Hz) was delivered to the left ALM.

(E and F) Behavioral comparisons with (blue) and without (black) photostimulation. (E) Detection probability (n = 16 sessions from four mice, mean ± SEM; two-way repeated-measure ANOVA with Tukey–Kramer post hoc comparisons, ***p = 4.5×10^{-5} for 0, *p = 0.037 for θ). (F) Reaction times for threshold and salient stimuli (n = 16 sessions from four mice, mean ± SEM; two-way repeated-measure ANOVA with Tukey–Kramer post hoc comparisons, *p = 0.012 for θ; *p = 0.036 for 2θ).

(G) Lick responses to brief photostimulation (three pulses at 20 Hz) in catch trials in a representative session.

(H) Lick responses to brief photostimulation averaged across sessions in trained expert mice (n = 10 sessions from five mice, mean ± SEM; left) and untrained naive mice (n = 10 sessions from five mice, mean ± SEM; right).

(I) Impact of brief photostimulation during ongoing licking in hit trials in expert mice (n = 10 sessions from five mice, mean ± SEM).

See also Figure S4.

KEY RESOURCES TABLE

REAGENT or RESOURCE	SOURCE	IDENTIFIER
Antibodies		
Chicken anti-GFP	GeneTex	Cat# GTX13970
Donkey anti-chicken, Alexa Fluor 488	Jackson ImmunoResearch	Cat# 703–545-155
Bacterial and Virus Strains		
AAV2/1-Syn-GCaMP6s-WPRE	Addgene	Cat# 100843-AAV1
AAV2/1-hSyn1-hM4D(Gi)-mCherry-WPRE	Viral Vector Facility UZH	Cat# v107–1
AAV2/1-hSyn-ChR2(H134R)-YFP-WPRE	Addgene	Cat# 26973-AAV1
AAV2/1-hSyn-ChR2(H134R)-YFP-2a-hM4Di-WPRE	Charité Viral Core Facility	N/A
Chemicals, Peptides, and Recombinant Proteins		
Alexa Fluor 647-conjugated streptavidin	Thermo Fisher Scientific	Cat# S32357
NucBlue	Thermo Fisher Scientific	Cat# R37606
Clozapine *N*-oxide	Tocris Bioscience	Cat# 4936
Muscimol	Tocris Bioscience	Cat# 0289
Muscimol, BODIPY TMR-X conjugate	Thermo Fisher Scientific	Cat# M23400
Deposited Data		
Dataset and Matlab analysis code	This study	https://doi.org/10.5281/zenodo.5036596
Experimental Models: Organisms/Strains		
Mice: C57BL/6J	Charles River	N/A
Software and Algorithms		
MATLAB	Mathworks	https://www.mathworks.com/products/matlab.html
ImageJ	NIH	https://imagej.nih.gov/ij/
IGOR Pro	WaveMetrics	https://www.wavemetrics.com/
Spike2	CED	http://ced.co.uk/products/spkovin
Wave Clus	[43]	https://www2.le.ac.uk/centres/csn/software/wave-clus